

Mass Estimators in the *Gaia* era

J. An¹, N. W. Evans², and A. J. Deason²

¹National Astronomical Observatories, Chinese Academy of Sciences, A20 Datun Road, Chaoyang District, Beijing 100012, PR China;*

²Institute of Astronomy, University of Cambridge, Madingley Road, Cambridge CB3 0HA.†

Accepted. Received 18 February 2022; in original form 13 October 2011

ABSTRACT

Forthcoming astrometric missions such as the *Gaia* satellite will bring to the fore the problem of estimating the enclosed mass from a set of positions, radial velocities and proper motions of tracer stars. Here, we show how to construct the tracer mass estimator when the proper motion data are available in addition to the usual line-of-sight velocity data. Notably, the mass estimators do not require any assumption on the anisotropy, as it is naturally incorporated through the different components of proper motions. In addition, the separate treatment of the proper motions and the line-of-sight velocities is desirable because they are observationally independent and thus the propagation of the combined uncertainties is rather straightforward. The extension to projected data is also sketched, together with a possible application of measuring the masses of Galactic globular clusters.

Key words: galaxies: fundamental parameters – galaxies: general – galaxies: haloes – galaxies: kinematics and dynamics – dark matter

1 INTRODUCTION

The great era of Galactic Cartography is upon us. The last twenty years have seen ambitious photometric and spectroscopic surveys of the Galaxy provide magnitudes and radial velocities for many millions of stars. Astrometric surveys of the Galaxy began with the now comparatively modest *Hipparcos* mission (see Perryman 2009 for a summary of its achievements) and will culminate with the launch of the *Gaia* satellite in 2013. This will provide micro-arcsecond astrometry for $\sim 10^9$ stars brighter than $G \approx 20$ (Perryman et al. 2001; Turon et al. 2005), as well as radial velocities for stars brighter than $G \approx 17$. Positional and kinematic data on bright stars in the Galaxy and its neighbours will be routinely available by the end of its mission.

This wealth of new data motivates the study of new theoretical questions. A classical problem in dynamical astronomy is to estimate the enclosed mass from the relative positions and velocities of a collection of bound test particles or tracers. Hitherto, work has primarily concentrated on the case in which the velocities are line-of-sight or projected. Here there has been an extensive body of work starting with methods essentially exploiting the virial theorem (Page 1952; Limber & Mathews 1960). The problems with such virial estimators were enunciated by Bahcall & Tremaine (1981), who introduced the notion of projected mass estimators based on sums of the projected mass contributions, namely $[(\text{projected distance}) \times (\text{radial velocity})^2 / G]$. In this form, the estimator is naturally suited to the case of a point mass (the Kepler potential). The extension to scale-free potentials with $\psi \propto r^{-\alpha}$ was developed by

White (1981), Evans et al. (2003) and Watkins et al. (2010, hereafter WEA). The estimator then takes a different form, namely sums of contributions of the form $[(\text{distance})^\alpha \times (\text{radial velocity})^2 / G]$. Finally, An & Evans (2011, hereafter Paper I) have shown how to adapt these ideas for an arbitrary spherical potential by choosing a weight function.

The case of proper motions has so far received very little attention. The coming of age of *Gaia* will make the availability of proper motions and radial velocities standard for all objects in the nearby Universe brighter than $G \approx 20$. Hence, this paper is devoted to the problem of estimating the enclosed mass from a tracer population when their space velocities are known.

2 TRACER MASS ESTIMATORS

Throughout this paper, we operate under the simplest assumption that the gravitational potential is spherical. A tracer population of stars with a number density ν resides in the potential. This is sampled to provide N_{tot} objects with known positions, radial velocities and proper motions. We shall usually consider the application to the problem of estimating the dark halo mass within the radius of the outermost datapoint r_{out} .

We start with the spherical Jeans equation, which reads

$$\frac{d(\nu\sigma_r^2)}{dr} + 2\beta\frac{\nu\sigma_r^2}{r} = -\nu\frac{GM}{r^2}, \quad (1)$$

where

$$\beta(r) = 1 - \frac{\sigma_\theta^2 + \sigma_\phi^2}{2\sigma_r^2} = 1 - \frac{\sigma_t^2}{2\sigma_r^2}, \quad (2)$$

* E-mail: jinan@nao.cas.cn

† E-mail: nwe,ajd75@ast.cam.ac.uk

is the Binney (1980) anisotropy parameter. This can be integrated into the form (see Paper I, eq. 11)

$$GM_{\text{out}} = \left\langle [3 + \hat{\alpha}(r) - 2\beta(r)] \frac{rv_r^2}{\tilde{\mu}} \right\rangle - 3r_{\text{out}}\zeta^2, \quad (3)$$

where the angled bracket represents the average over the whole tracer population. Here M_{out} is the total halo mass within radius r_{out} , and

$$\tilde{\mu}(r) \equiv \frac{M(r)}{M_{\text{out}}} \quad (0 \leq r \leq r_{\text{out}}) \quad (4)$$

is the halo mass profile $M(r)$ normalized by the total mass such that $\tilde{\mu}(r_{\text{out}}) = 1$, whereas

$$\hat{\alpha}(r) \equiv -\frac{d \log[r^{-1}M(r)]}{d \log r} = 1 - \frac{d \log \tilde{\mu}(r)}{d \log r}, \quad (5)$$

is the effective index for the gravitational potential. Finally, the surface term is given by

$$\zeta^2 \equiv \frac{\nu(r_{\text{out}})\sigma_r^2(r_{\text{out}})}{\bar{\nu}_{\text{out}}}; \quad \bar{\nu}_{\text{out}} \equiv \frac{3N_{\text{tot}}}{4\pi r_{\text{out}}^3}. \quad (6)$$

Note that $\bar{\nu}_{\text{out}}$ is the mean number density of the tracers in the sphere of the radius of r_{out} .

Next, we observe from equation (2) that

$$\left\langle \frac{rv_t^2}{\tilde{\mu}} \right\rangle = \frac{4\pi}{N_{\text{tot}}} \int_0^{r_{\text{out}}} \frac{\nu\sigma_t^2 r^3}{\tilde{\mu}} dr = \left\langle 2(1 - \beta) \frac{rv_t^2}{\tilde{\mu}} \right\rangle \quad (7)$$

where $v_t = (v_\theta^2 + v_\phi^2)^{\frac{1}{2}}$ is the tangential velocity and $\sigma_t = (\sigma_\theta^2 + \sigma_\phi^2)^{\frac{1}{2}}$ is the corresponding velocity dispersion. Hence, equation (3) is equivalent to

$$GM_{\text{out}} = \left\langle \frac{(1 + \hat{\alpha})rv_r^2}{\tilde{\mu}} \right\rangle + \left\langle \frac{rv_t^2}{\tilde{\mu}} \right\rangle - 3r_{\text{out}}\zeta^2, \quad (8)$$

which is our desired result expressing the mass M_{out} in terms of averages of observables.

The same can also be derived by directly integrating equation (1) whose left side reduces to

$$\frac{d(\nu\sigma_r^2)}{dr} + (2\sigma_r^2 - \sigma_t^2) \frac{\nu}{r} = \frac{1}{r^2} \frac{d(r^2\nu\sigma_r^2)}{dr} - \frac{\nu\sigma_t^2}{r}. \quad (9a)$$

With an arbitrary weight $h = h(r)$, this then results in

$$\int_0^{r_{\text{out}}} dr hr^2 \frac{d(r^2\nu\sigma_r^2)}{dr} - \int_0^{r_{\text{out}}} dr h\nu\sigma_t^2 r^3 = - \int_0^{r_{\text{out}}} dr h\nu GM r^2. \quad (9b)$$

The first integral here reduces to

$$\begin{aligned} \int_0^{r_{\text{out}}} dr hr^2 \frac{d(r^2\nu\sigma_r^2)}{dr} &= hr^4\nu\sigma_r^2 \Big|_0^{r_{\text{out}}} - \int_0^{r_{\text{out}}} dr r^2\nu\sigma_r^2 \frac{d(hr^2)}{dr} \\ &= hr^4\nu\sigma_r^2 \Big|_0^{r_{\text{out}}} - \int_0^{r_{\text{out}}} dr \frac{d \log(hr^2)}{d \log r} h\nu\sigma_r^2 r^3 \end{aligned} \quad (9c)$$

through integration by parts. Given that the inner boundary term $hr^4\nu\sigma_r^2|_0 = 0$ vanishes, replacing the first integral in equation (9b) by equation (9c) and multiplying the result by $4\pi N_{\text{tot}}^{-1}$, we find that

$$\langle hGM \rangle = \left\langle \left(2 + \frac{d \log h}{d \log r} \right) hr\nu\sigma_r^2 \right\rangle + \langle hr\nu\sigma_t^2 \rangle - 3r_{\text{out}}\zeta^2 h(r_{\text{out}}). \quad (10)$$

We recover equation (8) by choosing $h = \tilde{\mu}^{-1}$ since $d \log h / d \log r = -d \log \tilde{\mu} / d \log r = \hat{\alpha} - 1$.

2.1 Power-Law Weight

2.1.1 Scale-free potentials

Evans et al. (2011, hereafter EAD) have demonstrated that for most practical purposes adopting the scale-free assumption is a good approximation for choosing the proper mass estimator. This amounts to assuming that the mass model is given by

$$\tilde{\mu}(r) = \left(\frac{r}{r_{\text{out}}} \right)^{1-\alpha} \quad (0 \leq r \leq r_{\text{out}}), \quad (11)$$

and so $\hat{\alpha} = \alpha$ is constant. The exact models of the Kepler potential (a central point mass), the logarithmic potential (a truncated singular isothermal sphere), and the harmonic potential (a uniform homogeneous sphere) correspond to the cases that $\alpha = 1$, $\alpha = 0$, and $\alpha = -2$, respectively. With the mass model of equation (11), equation (8) reduces to

$$\frac{GM_{\text{out}}}{r_{\text{out}}^{1-\alpha}} = (1 + \alpha) \langle v_r^2 r^\alpha \rangle + \langle v_t^2 r^\alpha \rangle - 3r_{\text{out}}^\alpha \zeta^2. \quad (12)$$

Given that the tracer density profile essentially vanishes at finite r_{out} , the surface term should drop out (unless they are pressure-confined with a hard cut-off). Alternatively, following WEA, the surface term may be explicitly solved under the assumption of exact power-law behaviour for the tracer density ($\nu \propto r^{-\gamma}$) and the velocity dispersions, although strictly speaking the resulting solutions cannot be physical everywhere. It follows that β is constant since the Jeans equation implies that σ_r^2 , σ_t^2 , and GMr^{-1} all follow the same power-law. Therefore we can solve for $\nu(r_{\text{out}})/\bar{\nu}_{\text{out}} = \frac{1}{3}(3 - \gamma)$ and $\sigma_r^2 = (\gamma - 2\beta + \alpha)^{-1} GMr^{-1}$. If we substitute these for the surface term, then we find that:

$$\frac{GM_{\text{out}}}{r_{\text{out}}} + 3\zeta^2 = \frac{3 - 2\beta + \alpha}{\gamma - 2\beta + \alpha} \frac{GM_{\text{out}}}{r_{\text{out}}}. \quad (13)$$

Together with $\langle v_t^2 r^\alpha \rangle = 2(1 - \beta)\langle v_r^2 r^\alpha \rangle$, equation (12) results in

$$\frac{GM_{\text{out}}}{r_{\text{out}}^{1-\alpha}} = (\alpha + \gamma - 2) \langle v_r^2 r^\alpha \rangle + \langle v_t^2 r^\alpha \rangle. \quad (14)$$

This is equivalent to equations (16) and (24) of WEA if the anisotropy parameter is given by $\beta = 1 - \langle v_t^2 r^\alpha \rangle / (2\langle v_r^2 r^\alpha \rangle)$.

2.1.2 General cases

In reality, the scale-free mass model is a rather artificial abstraction. Never the less, equation (10) is actually valid for any mass profile and arbitrary weights. Hence with $h = r^{\tilde{\alpha}-1}$ and further assuming that the surface term vanishes as $r_{\text{out}} \rightarrow \infty$, we have that

$$G \langle r^{\tilde{\alpha}-1} M \rangle = (1 + \tilde{\alpha}) \langle v_r^2 r^{\tilde{\alpha}} \rangle + \langle v_t^2 r^{\tilde{\alpha}} \rangle. \quad (15)$$

We have used the symbol $\tilde{\alpha}$ to emphasize the fact that this needs not be the same as the power-law index of the potential. That is to say, the scale-free estimator on the right-hand side actually returns the radial moments of any given (not necessarily scale-free) mass profile. Although it is clear that the left-hand side is directly related to the total mass, the specific constant factor associated with it in general depends on both the mass profile and the tracer density profile. There are some exceptions that are worthy of note here. The first is the case of the power-law mass profile with $\alpha = \tilde{\alpha}$, for which $\langle r^{\tilde{\alpha}-1} M(r) \rangle = \langle r_{\text{out}}^{\alpha-1} M_{\text{out}} \rangle = r_{\text{out}}^{\alpha-1} M_{\text{out}}$ is constant regardless of the tracer density profile. The second is the self-consistent gravitating

Table 1. Mean values $\langle v_r^2 r^\alpha \rangle$ for satellites in Table 1 of WEA.

r_{out}	300 kpc	200 kpc ($\times 10^{11} M_\odot$)	100 kpc
$G^{-1} r_{\text{out}}^{1-\alpha} \langle v_r^2 r^\alpha \rangle$	2.86 ± 0.87	1.75 ± 0.40	1.20 ± 0.22
(w/o Leo I)	2.09 ± 0.42		
(w/o Leo I, Her)	1.76 ± 0.27	1.45 ± 0.28	

Here $\alpha = 0.55$ following WEA. Only satellites within $r \leq r_{\text{out}}$ are counted. These consist of 14 satellites with $r_{\text{out}} = 100$ kpc, 21 (including Her) with $r_{\text{out}} = 200$ kpc, and 24 (including Leo I and Her) with $r_{\text{out}} = 300$ kpc. The quoted uncertainties, which range from ~ 15 to $\sim 30\%$, are purely due to the scatter, i.e., $\sigma/N^{1/2} = s/\sqrt{N-1}$ where σ^2 and s^2 are the unbiased and biased sample variance estimate and N is the number of data points.

system for which the $\tilde{\alpha} = 1$ case results in

$$\begin{aligned} \langle M \rangle &= \frac{4\pi}{N_{\text{tot}}} \int_0^\infty dr \, v r^2 M = \frac{1}{M_{\text{tot}}} \int_0^\infty dr \, \frac{dM}{dr} M \\ &= \frac{1}{2M_{\text{tot}}} \int_0^\infty dr \, \frac{dM^2}{dr} = \frac{M_{\text{tot}}}{2} \end{aligned} \quad (16)$$

because $dM/dr = 4\pi v^2 \rho$ where ρ is the mass density and the ratio $\rho/v = M_{\text{tot}}/N_{\text{tot}}$ is constant. (By contrast, for a central M_\bullet point-mass, we would have $\langle M \rangle = \langle M_\bullet \rangle = M_\bullet$.) An additional general result deduced from equation (15) is for $\tilde{\alpha} = 0$, that is,

$$\left\langle \frac{GM}{r} \right\rangle = \langle v_r^2 \rangle + \langle v_t^2 \rangle = \langle v^2 \rangle, \quad (17)$$

which is simply the scalar virial theorem for a spherical system.

3 THE MASS OF THE MILKY WAY

3.1 Present Proper Motions of the Satellites

WEA have used combinations of the averages in the form of $\langle v_r^2 r^\alpha \rangle$ and $\langle v^2 r^\alpha \rangle = (3 - 2\beta) \langle v_r^2 r^\alpha \rangle$ to estimate the mass of the Galaxy from the kinematics of its satellites including their proper motions. Whilst their approach of incorporating proper motions has a valid justification in that the anisotropy value derived by combining the line-of-sight (los) and proper motions appears to be severely biased towards tangential motions, it is still instructive to use the consistent mass estimator without a priori assumptions on the anisotropy.

Here we use equation (14) to combine the los and proper motion data gathered in WEA and estimate the Galactic mass. We first note the scaling relation for observable combinations of kinematic properties ($\mu\text{as a}^{-1} \equiv \text{micro-arcseconds per year}$):

$$\begin{aligned} \frac{v_r^2 r^\alpha}{G r_{\text{out}}^{\alpha-1}} &= 2.325 \cdot 10^9 M_\odot \left(\frac{r_{\text{out}}}{100 \text{ kpc}} \right)^{1-\alpha} \left(\frac{r}{100 \text{ kpc}} \right)^\alpha \left(\frac{v_\ell}{10 \text{ km s}^{-1}} \right)^2; \\ \frac{v_t^2 r^\alpha}{G r_{\text{out}}^{\alpha-1}} &= 5.225 \cdot 10^8 M_\odot \left(\frac{r_{\text{out}}}{100 \text{ kpc}} \right)^{1-\alpha} \left(\frac{r}{100 \text{ kpc}} \right)^{\alpha+2} \left(\frac{\mu}{10 \mu\text{as a}^{-1}} \right)^2. \end{aligned} \quad (18)$$

Here, v_ℓ and μ are the los velocity and the proper motion of the satellite, respectively. For the satellites considered here, the Galactocentric distances are large enough to ignore the sun being off-centre in the Galaxy. We shall therefore assume that $v_r = v_\ell$ and $v_t = r\mu$, and the use of equation (14) is appropriate.

Table 1 lists the contribution to equation (14) of the radial motions of satellites assembled in Table 1 of WEA with $\alpha = 0.55$, which is the ‘best-fitting’ value of the power-law index to the potential

Table 2. Numerical contribution to the proper motion mass estimator $G^{-1} r_{\text{out}}^{1-\alpha} v_t^2 r^\alpha$ for satellites in Table 4 of WEA.

r_{out}	200 kpc ($\times 10^{11} M_\odot$)	100 kpc ($\times 10^{11} M_\odot$)
Car	5.3 ± 3.6	
Dra	90.6 ± 47.1	66.3 ± 34.5
For	60.6 ± 9.4	
MCs	48.5 ± 2.4	35.5 ± 1.8
Scl	0.43 ± 1.20	0.31 ± 0.88
Sex	4.1 ± 12.2	3.0 ± 9.0
UMi	10.9 ± 6.7	8.0 ± 4.9

Here again $\alpha = 0.55$. All listed satellites have $r < 100$ kpc except for Carina ($r = 102$ kpc) and Fornax ($r = 140$ kpc). For the Magellanic Clouds, we choose $r = 50$ kpc for the barycentre (assuming the mass ratio of LMC/SMC ~ 11). The quoted errors are the directly propagated uncertainties of the proper motion measurements assuming no correlation between the two components of the proper motions.

of a typical NFW halo as determined by WEA. The uncertainties quoted are purely statistical and typically of about ~ 20 per cent, comparable to ~ 25 per cent derived via Monte Carlo simulations in WEA. Assuming isotropy and adopting the tracer power-law slope $\gamma = 2.6$, the Galactic mass based on these data can be estimated by multiplying these by a factor of 3.15, the results of which basically reproduce those reported in Table 3 of WEA.

Table 2 on the other hand provides us with the individual contributions to the mass estimator of the proper motions measured for seven Galactic satellites reported in Table 4 of WEA. In contrast to the los velocities, the uncertainties associated with each measurement are rather large. This not only contributes additional uncertainties in the final mass estimate, but also complicates the proper weighting scheme appropriate for the average related to the mass estimator. In Table 3, we present the result calculated with equation (14). For the average of the proper motion contributions, the results based on both the unweighted arithmetic mean and the mean weighted by the reciprocal of the observational variance (i.e., σ^{-2} where σ is the associated uncertainty reported in Table 2) are given. Compared to the results based on the los motions alone, the final statistical uncertainties are quite larger ranging from ~ 50 per cent to a factor of two. More seriously, the results vary in significant amounts depending on the weighting scheme and the choice of outliers (which may be due to observational errors and/or true unbound objects), although they are formally consistent with one another given large error bars. It appears that the safest conclusion that can be drawn at this point is that the existing proper motion data do not provide any meaningful discriminating information on the mass of the Milky Way without any a priori assumption on the motions of the Galactic satellites as a whole or the particular target.

3.2 The Age of Gaia

Let us now estimate the benefits that *Gaia* will bring. We do this by constructing mock datasets of los velocities and proper motions for sets of dwarf galaxy satellites extracted from a suite of simulations, the *Galaxies-Intergalactic Medium Interaction Calculation*, which are described in detail in Crain et al. (2009). They consist of a set of hydrodynamical resimulations of five nearly spherical regions ($\sim 20 h^{-1}$ Mpc in radius) extracted from the *Millennium Simulation* (Springel et al. 2005). Deason et al. (2011) extracted a set of

Table 3. Mass of the Milky Way

r_{out}	200 kpc (w/o Her)		100 kpc
unweighted	33.5 ± 15.4	33.2 ± 15.4	24.0 ± 14.9
(w/o Dra)	23.7 ± 11.1	23.3 ± 11.1	13.1 ± 8.6
(w/o MCs)	30.7 ± 17.9	30.4 ± 17.9	20.8 ± 18.8
(w/o Dra, MCs)	18.3 ± 11.9	18.0 ± 11.9	5.2 ± 4.8
σ^{-2} -weighted	12.1 ± 10.6	11.8 ± 10.6	8.6 ± 10.4
(w/o Dra)	12.1 ± 11.4	11.8 ± 11.4	8.6 ± 11.6
(w/o MCs)	4.1 ± 6.5	3.8 ± 6.5	2.0 ± 4.9
(w/o Dra, MCs)	4.1 ± 6.8	3.7 ± 6.8	2.0 ± 4.2

The estimator uses equation (14) with $\alpha = 0.55$ and $\gamma = 2.6$. The mass is in the units of $10^{11} M_{\odot}$. The uncertainties are purely statistical incorporating both scatters and the measurement uncertainties found in Table 2.

galaxies that resemble the Milky Way. The catalogue consists of 431 parent haloes and 4864 associated satellite galaxies.

The mass estimators provide the total mass within the radius of the farthest tracer ($\approx r_{\text{out}}$). We compute the ‘true’ mass within the virial radius of each halo and compare to the masses found via our estimator. We use all satellites, but check that our results are not significantly affected when only luminous satellites are included. Figure 1 refers to data sets of radial velocities and true distances (dashed histogram), and radial velocities, proper motions and projected distances (solid histogram). An uncertainty of $100 \mu\text{as a}^{-1}$ for each star is assumed; for comparison, *Gaia*’s targeted accuracies are $10 \mu\text{as a}^{-1}$ at $G \sim 15$ and $150 \mu\text{as a}^{-1}$ at $G \sim 20$ (Lindgren et al. 2008). For each tangential velocity measurement, a Gaussian distribution centred on the ‘real measurement’ with error is derived from the proper motion (and so depends on distance). For each satellite, it is assumed that *Gaia* will detect 100 stars, which is reasonable enough for the case of the satellites of the Milky Way (Wilkinson & Evans 1999). The left panel of Figure 1 uses the estimator given by equation (14), the right panel uses equation (12) neglecting the surface term.

We quantify the improvement by means of two statistical measures as originally introduced by EAD. First, we define the Fraction of Reasonable Estimates (FRE) as the fraction of estimates within the factor of two of the true mass (see also Deason et al. 2011). We also give the Inter Quartile Range (IQR) of the mass estimates, which gives a good indication of the spread. We see that at *Gaia*’s accuracy, the proper motions can contribute significantly to an improved estimate of the mass of the Milky Way. Even with the small number of satellites, the inclusion of proper motion data via the estimator of equation (14) means that 93 per cent of estimates are within a factor of two, as opposed to 82 per cent with radial velocities alone. The solid histogram is also more narrow than the dashed, as indicated by a smaller IQR of $-0.05 < \log(M_{\text{est}}/M_{\text{true}}) < 0.09$. Notice from the right panel that the estimator of equation (12) also performs very well with regard to the FRE, but the neglect of the boundary term causes an offset so the estimator is biased.

As is noted by EAD, there are a number of ways in which mock catalogues from simulations differ from the assumptions used to derive the estimators. For example, dark haloes are not generally spherical, infall continues to the present day, and the observed satellites are not necessarily virialized and well-described by an equilibrium distribution. Therefore the performance of the mass estimators is very encouraging.

4 PROJECTED DATA WITH PROPER MOTIONS

In most practical cases, the kinematic data available are limited by projection. Hence, the naturally observable velocity dispersions are those along the line of sight and of proper motions. In addition, for most dynamical systems of interest, their spatial extents are typically much smaller than their distances from us as a whole. On the positive side, this indicates that, from the observer’s perspective, the observed los velocities v_{ℓ} basically correspond to the coordinate velocity component v_z if we have chosen the cylindrical polar coordinate centred at the centre of the tracer population and the positive z -axis running from the centre to the observer. In addition, the remaining two orthogonal components of the velocity $\mathbf{v}_{\phi} = (v_R, v_{\phi})$ are linearly proportional to the two components of the proper motion with $\mathbf{v}_{\phi} = s\boldsymbol{\mu}$ where s is the distance to the system as a whole and $\boldsymbol{\mu}$ is the proper motion vector.

On the negative side however, the radial distance of any individual tracer to the centre of the system is very difficult to determine precisely. In particular, since the absolute uncertainty (δr) of the radial distance (r) measurement is in the same order as the uncertainty (δs) of the individual distance (s) measurement, i.e., $\delta r \sim \delta s$ (NB., the error in the distance measurement typically dominates that in the angular separation whilst the precise determination of the distance to the centre only improves the precision by $\sim \sqrt{2}$), the fractional uncertainty of the radial distance is roughly estimated to be $(\delta r/r) \sim (\delta s/s)(s/r) \sim (\delta s/s)/\varphi$ where $\varphi \sim r/s$ is of order the angular extent of the system. In other words, ~ 10 per cent estimates of the radial distances for tracers in a degree-sized system require the individual distance measurement in a better than ~ 0.2 per cent precision. Consequently, the distance handle associated with the tracer is likely to be limited to the projected (linear or angular, depending on whether the distance to the system as a whole is known or not) separation. In the following, we develop the projected mass estimators similar to those of Bahcall & Tremaine (1981) and Heisler et al. (1985) using v_{ℓ} and R as observables but further augmented by including the transverse velocity \mathbf{v}_{ϕ} derived from the proper motion. We note that this problem has been partly addressed by Leonard & Merritt (1989).

4.1 The Projected Mass Estimator with Transverse Velocities

Let us first consider the coordinate system with its origin located at the centre of the system and the positive z -axis running from the origin to us. Then, the tracer velocity components in the spherical polar coordinate $(v_r, v_{\theta}, v_{\phi})$ transform to those in the cylindrical coordinate (v_R, v_{ϕ}, v_z) according to

$$v_R = v_r \sin \theta + v_{\theta} \cos \theta; \quad v_z = v_r \cos \theta - v_{\theta} \sin \theta. \quad (19)$$

If the tracers are described by a generic two-integral distribution that is non-rotating and spherically symmetric, then the velocity dispersion tensor is diagonalized in the spherical polar coordinate with $\sigma_{\theta\theta} = \sigma_{\phi\phi}$. These transform to the velocity dispersion tensor in the cylindrical polar coordinate via

$$\begin{aligned} \sigma_{RR}^2 &= \sigma_r^2 \sin^2 \theta + \sigma_{\theta}^2 \cos^2 \theta = (1 - \beta \cos^2 \theta) \sigma_r^2 \\ \sigma_{\phi\phi}^2 &= \sigma_{\theta}^2 = (1 - \beta) \sigma_r^2 \\ \sigma_{zz}^2 &= \sigma_r^2 \cos^2 \theta + \sigma_{\theta}^2 \sin^2 \theta = (1 - \beta \sin^2 \theta) \sigma_r^2 \\ \sigma_{Rz}^2 &= (\sigma_r^2 - \sigma_{\theta}^2) \sin \theta \cos \theta = \beta \sin \theta \cos \theta \sigma_r^2, \end{aligned} \quad (20)$$

where $\sigma_r^2 = \sigma_{rr}^2$ and $\sigma_{\theta}^2 = \sigma_{\theta\theta}^2$, and β is given by equation (2).

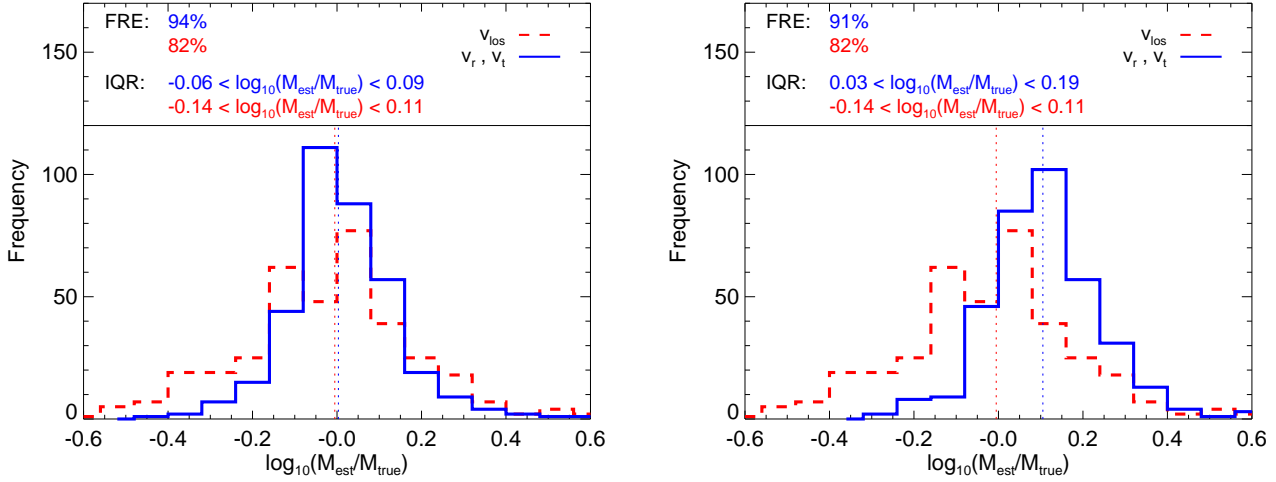


Figure 1. Left: Histograms showing the ratio of the estimated mass to the true mass for the two different mass estimators. The dashed histogram uses sets of radial velocities and distances with the tracer mass estimator of WEA. The solid histogram uses sets full space velocities and distances, with mass estimator of eq. (14). The FRE and IQR are the fraction of reasonable estimates and the inter-quartile range as defined in the text. The means of the distributions are shown by vertical dotted lines. Right: As the left panel, but now the solid histogram uses eq. (12) neglecting the surface term.

Using equation (20), it is trivial to find for $\alpha > -2$ that

$$\begin{aligned} \langle v_R^2 R^\alpha \rangle &= \frac{2\pi}{N_{\text{tot}}} \int_0^\infty dr r^2 v(r) \int_0^\pi d\theta \sin \theta \sigma_{RR}^2 r^\alpha \sin \theta \\ &= \frac{2\pi}{N_{\text{tot}}} \int_0^\infty dr v r^{2+\alpha} (\sigma_r^2 B_{2+\frac{\alpha}{2}, \frac{1}{2}} + \sigma_\theta^2 B_{1+\frac{\alpha}{2}, \frac{3}{2}}) \\ &= B_\alpha [(2+\alpha) \langle v_r^2 r^\alpha \rangle + \langle v_\theta^2 r^\alpha \rangle] \end{aligned} \quad (21a)$$

$$\langle v_\phi^2 R^\alpha \rangle = (3+\alpha) B_\alpha \langle v_\theta^2 r^\alpha \rangle \quad (21b)$$

$$\langle v_z^2 R^\alpha \rangle = B_\alpha [\langle v_r^2 r^\alpha \rangle + (2+\alpha) \langle v_\theta^2 r^\alpha \rangle] \quad (21c)$$

where $B_{a,b} = \Gamma(a)\Gamma(b)/\Gamma(a+b)$ and $\Gamma(x)$ are the beta and gamma function and

$$B_\alpha \equiv \frac{1}{2} B_{1+\frac{\alpha}{2}, \frac{3}{2}} = \frac{\sqrt{\pi} \Gamma(1+\frac{\alpha}{2})}{4 \Gamma(\frac{5+\alpha}{2})}. \quad (21d)$$

The result extends to the $\alpha = -2$ case (homogeneous sphere) with

$$\begin{aligned} \langle v_X^2 \delta(R^2) \rangle &= \frac{2\pi}{N_{\text{tot}}} \int_{-\infty}^\infty dz \int_0^\infty dR R v \sigma_{XX}^2 \delta(R^2) \\ &= \frac{\pi}{N_{\text{tot}}} \int_{-\infty}^\infty dz v \sigma_{XX}^2 |_{R=0,z} \end{aligned} \quad (22a)$$

where $\delta(x)$ is the Dirac delta. Since $(R=0, z>0)$ and $(R=0, z<0)$ correspond to $(r=z, \theta=0)$ and $(r=|z|, \theta=\pi)$, we find from equation (20) that

$$\begin{aligned} \langle v_R^2 \delta(R^2) \rangle &= \frac{2\pi}{N_{\text{tot}}} \int_0^\infty dr v \sigma_\theta^2 = \frac{1}{2} \langle v_\theta^2 r^{-2} \rangle \\ \langle v_\phi^2 \delta(R^2) \rangle &= \frac{2\pi}{N_{\text{tot}}} \int_0^\infty dr v \sigma_\theta^2 = \frac{1}{2} \langle v_\theta^2 r^{-2} \rangle \\ \langle v_z^2 \delta(R^2) \rangle &= \frac{2\pi}{N_{\text{tot}}} \int_0^\infty dr v \sigma_r^2 = \frac{1}{2} \langle v_r^2 r^{-2} \rangle. \end{aligned} \quad (22b)$$

This result is identified with the formal limit of equation (21) as $\alpha \rightarrow -2^+$ once we note that $\lim_{\alpha \rightarrow -2^+} R^\alpha / \Gamma(1+\frac{\alpha}{2}) = \delta(R^2)$.

For an observer located sufficiently far away, the axial and sectional velocities are basically the los and the transverse velocities,

respectively. It follows that $\langle v_\ell^2 R^\alpha \rangle = \langle v_z^2 R^\alpha \rangle$ and

$$\langle v_\phi^2 R^\alpha \rangle = B_\alpha [(2+\alpha) \langle v_r^2 r^\alpha \rangle + (4+\alpha) \langle v_\theta^2 r^\alpha \rangle]. \quad (23)$$

If the two components of the transverse velocities are separately measurable, we can derive the right-hand of equation (15) from

$$(1+\alpha) \langle v_R^2 R^\alpha \rangle + \langle v_\phi^2 R^\alpha \rangle = (2+\alpha) B_\alpha [(1+\alpha) \langle v_r^2 r^\alpha \rangle + 2 \langle v_\theta^2 r^\alpha \rangle]. \quad (24a)$$

On the other hand, the same may be found by combining the los and the two-dimensional transverse velocity dispersions

$$\langle v_\phi^2 R^\alpha \rangle - \langle v_\ell^2 R^\alpha \rangle = B_\alpha [(1+\alpha) \langle v_r^2 r^\alpha \rangle + 2 \langle v_\theta^2 r^\alpha \rangle]. \quad (24b)$$

Directly substituting these in equation (15) then leads to

$$GB_\alpha \langle r^{\alpha-1} M \rangle = \frac{(1+\alpha) \langle v_R^2 R^\alpha \rangle + \langle v_\phi^2 R^\alpha \rangle}{2+\alpha} = \langle v_\phi^2 R^\alpha \rangle - \langle v_\ell^2 R^\alpha \rangle, \quad (25a)$$

which is again valid for $\alpha > -2$. We note that equation (25a) with $\alpha = -1, 0, 1, 2$ are already found in Leonard & Merritt (1989). If $\alpha = -2$, then strictly the average is not convergent, but using equation (22), we find the proper limiting equation, namely,

$$\frac{1}{2} G \langle r^{-3} M \rangle = \langle v_\phi^2 \delta(R^2) \rangle - \langle v_\ell^2 \delta(R^2) \rangle, \quad (25b)$$

whereas $\langle v_R^2 \delta(R^2) \rangle = \langle v_\phi^2 \delta(R^2) \rangle$. Provided that the distance s to the system as a whole is known independently, equation (25a) is the proper extension of the projected mass estimator to include the information from proper motions. Note that, if the vectorial dispersion of the proper motions is known, incorporating the los velocity dispersions in fact over-constrains the system under the assumption of the two-integral spherically-symmetric distribution.

4.1.1 Mass measurements of globular clusters

We can test these formulae in the context of applications. A possible class of targets would be nearby dwarf spheroidal/elliptical galaxies, similar to the examples found in EAD. However, the proper motion dispersion for an imaginary satellite of mass $10^7 M_\odot$ and radius 0.5 kpc located at 50 kpc is about $\sim 40 \mu\text{as a}^{-1}$. Even

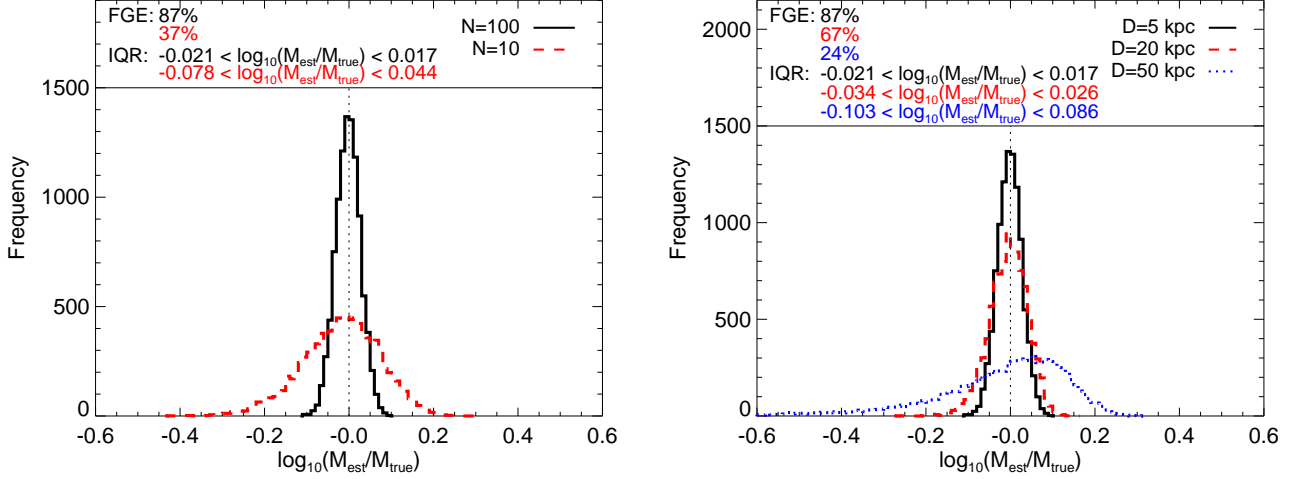


Figure 2. Left: Estimates of enclosed mass of a globular cluster using 10 (dashed) and 100 (solid) tracers from 10^5 Monte Carlo realizations. Proper motion errors of $100 \mu\text{as a}^{-1}$ and a distance of 5 kpc are assumed. Right: Estimates of enclosed mass as a function of globular cluster distance, namely 5 (solid), 20 (dashed) or 50 (dotted) kpc, assuming 100 stars can be measured per globular cluster. Model has parameters $\alpha = 0$ and $\gamma = 3$.

with *Gaia*, these will be challenging observations even if there exist large enough samples of sufficiently luminous tracers, which is itself unclear in any case. Alternatively, we can consider mass estimates of Galactic globular clusters. In fact, for a few bright clusters, there already exist very good internal proper motion data sets (e.g., Anderson & van der Marel 2010). Yet the existing data for these are sufficiently large and of high quality so that the complete dynamical modelling is technically feasible (see e.g., van der Marel & Anderson 2010) – note that there is no degeneracy involving anisotropy with the proper motion data incorporated. In principle, we may still utilize these for the projected mass estimator but its application is clearly didactic at best. Instead we investigate *Gaia*’s capability regarding possible applications of projected mass estimators for ‘typical’ globular clusters in varying distances.

In contrast to dwarf satellites, the main challenge of globular cluster observations is expected to be crowding, and so the choice of the tracer subsample is important for any practical application of mass estimators. Blue horizontal branch (BHB) stars have a *G*-band magnitude of about ~ 19 at 50 kpc. So, *Gaia* will be able to detect a BHB star out to 50 kpc and measure their proper motions with accuracies of better than $100 \mu\text{as a}^{-1}$. By contrast, radial velocities will usually be missing, as *Gaia*’s radial velocity spectrograph has a limiting magnitude of $G \approx 17$. Most globular clusters harbour significant populations of BHB stars (e.g., Brown et al. 2005), and so equation (25a) can be exploited to measure the mass of globular clusters in the Milky Way from proper motions provided by *Gaia*. To test the feasibility, we use the self-consistent distributions of power-law densities with $\rho \propto r^{-3}$ in logarithmic potentials (White 1981; Evans et al. 1997) to generate mock datasets of proper motions and projected distances, degraded with the *Gaia* errors. The estimated mass computed via equation (25a) can then be compared to the known true mass. Figure 2 shows the results of Monte Carlo simulations. In the left panel, the globular cluster is assumed to lie at a distance of 5 kpc and the sample size is 10 or 100 tracers with projected positions and proper motions. As the histograms are quite tight, we have replaced FRE with the Fraction of Good Estimates (FGE), where ‘Good’ means that the mass estimate is within 10 per cent of the true mass. We see that 10 tracers are too small for re-

liable results, but 100 tracers are ample. The right panel shows the estimated masses as a function of distance, with the globular cluster assumed to lie at 5, 20 and 50 kpc respectively. In each case, 100 tracers are used, and we see that the results are still acceptable at distances of 20 kpc, with 67 per cent of the mass estimates being good. With increasing distance, however, the accuracy degrades so that by 50 kpc, only 24 per cent of the estimates are good.

4.2 The Projected Mass Estimator with Proper Motions

Now we consider the case that the distance s is also unknown. It can in principle be measured by matching the *los* velocity and the proper motion dispersions. Specifically, the last equality of equation (25a) is rearranged to

$$(2 + \alpha) \langle v_\ell^2 R^\alpha \rangle = \langle v_R^2 R^\alpha \rangle + (1 + \alpha) \langle v_\phi^2 R^\alpha \rangle. \quad (26)$$

With $R = s\varphi$ and $v_\phi = s\mu$ where φ is the angular separation from the centre, the distance s is found from direct observables as in

$$s^2 = \frac{(2 + \alpha) \langle v_\ell^2 \varphi^\alpha \rangle}{\langle \mu_R^2 \varphi^\alpha \rangle + (1 + \alpha) \langle \mu_\phi^2 \varphi^\alpha \rangle}, \quad (27)$$

where μ_R and μ_ϕ are the radial and azimuthal projections of the proper motion. Note that the $\alpha = 0$ case reduces to $s^2 \langle \mu^2 \rangle = \langle v_\ell^2 \rangle$ irrespective of the anisotropy, which corresponds to the classical statistical parallax technique of measuring distance. This is because only in the $\alpha = 0$ case are the velocity distributions independent of position, which usually assumed in statistical parallax applications (see e.g., Trumpler & Weaver 1953).

At the same time, we can also solve for the anisotropy parameter

$$\beta_{\text{eff}} = 1 - \frac{\langle v_\ell^2 \varphi^\alpha \rangle}{\langle v_\ell^2 R^\alpha \rangle} = \frac{(3 + \alpha) [\langle \mu_R^2 \varphi^\alpha \rangle - \langle \mu_\phi^2 \varphi^\alpha \rangle]}{(3 + \alpha) \langle \mu_R^2 \varphi^\alpha \rangle + \langle \mu_\phi^2 \varphi^\alpha \rangle}. \quad (28)$$

The unique mass estimator that follows this is

$$GB_\alpha \langle r^{\alpha-1} M \rangle = \frac{(1 + \alpha) \langle \mu_R^2 \varphi^\alpha \rangle + \langle \mu_\phi^2 \varphi^\alpha \rangle}{\langle \mu_R^2 \varphi^\alpha \rangle + (1 + \alpha) \langle \mu_\phi^2 \varphi^\alpha \rangle} \langle v_\ell^2 R^\alpha \rangle \quad (29)$$

with $\langle v_\ell^2 R^\alpha \rangle = s^\alpha \langle v_\ell^2 \varphi^\alpha \rangle$. This again is in fact equivalent to equations (24) and (25) of Paper I with β replaced by equation (28) and the boundary term dropped. If one preferred the explicitly solved boundary term used in WEA, one might use their equations (26) and (27) with β replaced by the same equation (28). However, we note that estimators in equations (27)-(29) are likely to be biased if the sample means are used to estimate for the averages in the right-hand sides as these formulae involve a division by a mean whose corresponding dispersion is finite non-zero.

5 CONCLUSIONS

Hitherto, proper motion data have not normally been used in measurements of the mass of nearby galaxies like the Milky Way and M31. Proper motions are only available for a handful of satellites – namely, Carina, Draco, Fornax, Sculptor, Sextans, Ursa Minor and the Large and Small Magellanic Clouds for the Milky Way, together with IC10 and M33 for M31. As these are difficult measurements, the errors are often quite large. Additionally, agreement between different investigators regarding the proper motions for Ursa Minor (Scholz & Irwin 1994; Piatek et al. 2005) and Sculptor (Piatek et al. 2006; Walker et al. 2008) is poor. Therefore, there has been little attention given to their exploitation.

This situation is about to change. The *Gaia* satellite, to be launched in 2013, will measure the positions and proper motions of $\sim 10^9$ stars in our Galaxy and other members of the Local Group. The proper motions have a targeted accuracy of between $10 \mu\text{as a}^{-1}$ (at $G \sim 15$) and $150 \mu\text{as a}^{-1}$ (at $G \sim 20$). This therefore motivates detailed study of the use of proper motions in mass estimators. Particularly in the case of the Milky Way, the proper motions are crucial as the line-of-sight velocity closely coincides with the radial velocity as measured from the Galactic Centre. Hence, proper motions provide new information on the velocity anisotropy that is not available in the line-of-sight velocities alone.

Here we have shown how to solve the classical problem of estimating the enclosed mass from the positions and space velocities of a set of tracers. The main result is equation (8), which shows how to compute the enclosed mass in terms of averages over the observable velocity components for a given halo mass model. If, as is reasonable, we use a scale-free assumption for the dark halo, then the mass estimator reduces to equation (14). Note values of $\alpha \sim 0.5$ for the power-law index for the potential are good approximations to the NFW halo (Deason et al. 2011; Evans et al. 2011).

We have used these new formulae to demonstrate that the existing proper motion data for the Milky Way satellites provide no meaningful discriminating information on the mass of the Milky Way. This though will change in the era of *Gaia*. Using mock catalogues of satellites extracted from the simulations, we have shown that our new mass estimator, when equipped with proper motions with the targeted *Gaia* accuracies, significantly outperforms the estimator used with line-of-sight velocities only. We have also given the extension of the formulae to the instances where projected positions and proper motions are available. These formulae provide a feasible method for the *Gaia* satellite to measure the internal masses of Milky Way globular clusters lying within 20 kpc.

As is usual for a spherical system, we have assumed no rotation in the tracer population for our derivation of the mass estimators. (Clearly, any rotating population cannot be spherically symmetric although it may be spherical in density.) However, the tracer velocities in our formulae appear as their second moments rather than the dispersions/variances (in the rest frame of the potential). That is,

once the bulk *linear* motion of the tracers is subtracted, the estimators actually do not distinguish between the random and coherent motions of the tracers. Hence, we argue that the formulae as they are are still valid even if the population is in fact supported through the mixture of the pressure and the rotation.

ACKNOWLEDGMENTS

This paper incorporates works carried out during the first author's visit to the IoA (Cambridge), 2011 September, which was in part supported by the IoA's visitor grant. JA is supported by the Chinese Academy of Sciences (CAS) Fellowships for Young International Scientist, grant no. 2009Y2AJ7 and the National Natural Science Foundation of China (NSFC) Research Fund for International Young Scientist. AJD thanks the Science and Technology Facilities Council (STFC; UK) for the award of a studentship.

REFERENCES

- An J. H., Evans N. W., 2011, MNRAS, 413, 1744 (Paper I)
- Anderson J., van der Marel R. P., 2010, ApJ, 710, 1032
- Bahcall J. N., Tremaine S., 1981, ApJ, 244, 805
- Binney J., 1980, MNRAS, 190, 873
- Brown W. R., Geller M. J., Kenyon S. J., Kurtz M. J., Allende Prieto C., Beers T. C., Wilhelm R., 2005, AJ, 130, 1097
- Crain R. A., et al., 2009, MNRAS, 399, 1773
- Deason A. J., McCarthy I. G., Font A. S., Evans N. W., Frenk C. S., Belokurov V., Libeskind N. I., Crain R. A., Theuns T., 2011, MNRAS, 415, 2607
- Evans N. W., Häfner R. M., de Zeeuw P. T., 1997, MNRAS, 286, 315
- Evans N. W., Wilkinson M. I., Perrett K. M., Bridges T. J., 2003, ApJ, 583, 752
- Evans N. W., An J., Deason A. J., 2011, ApJ, 730, L26 (EAD)
- Heisler J., Tremaine S., Bahcall J. N., 1985, ApJ, 298, 8
- Leonard P. J. T., Merritt D., 1989, ApJ, 339, 195
- Limber D. N., Mathews W. G., 1960, ApJ, 132, 286
- Lindegren L., et al., 2008, in Jin J., Platais I., Perryman M.A.C., eds, Proc. IAU Symposium No. 248, A Giant Step: from Milli- to Micro-arcsecond Astrometry: Cambridge Univ. Press, Cambridge, p.217
- Page T., 1952, ApJ, 116, 63
- Perryman M. A. C., de Boer K. S., Gilmore G., Høg E., Lattanzi M. G., Lindegren L., Luri X., Mignard F., Pace O., de Zeeuw P. T., 2001, A&A, 369, 339
- Perryman M., 2009, Astronomical Applications of Astrometry: Ten Years of Exploitation of the *Hipparcos* Satellite Data. Cambridge Univ. Press, Cambridge
- Piatek S., Pryor C., Bristow P., Olszewski E. W., Harris H. C., Mateo M., Minniti D., Tinney C. G., 2005, AJ, 130, 95
- Piatek S., Pryor C., Bristow P., Olszewski E. W., Harris H. C., Mateo M., Minniti D., Tinney C. G., 2006, AJ, 131, 1445
- Scholz R. D., Irwin M. J., 1994, in MacGillivray H.T., Thomson E.B., Lasker B.M., Reid I.N., Malin D.F., West R.M., Lorenz H., eds, Proc. IAU Symposium No. 161, Astronomy from Wide-Field Imaging: Kluwer Academic Publ., Dordrecht, p.535
- Springel V., et al., 2005, Nature, 435, 629
- Trumpler R. J., Weaver H. F., 1953, Statistical Astronomy. Univ. of California Press, Berkeley (REPRINTED 1962, Dover Publ., New York)
- Turon C., O'Flaherty K. S., Perryman M. A. C., 2005, Proc. the *Gaia* Symposium "The Three-Dimensional Universe with *Gaia*". European Space Agency Publ.
- van der Marel R. P., Anderson J., 2010, ApJ, 710, 1063
- Walker M. G., Mateo M., Olszewski E. W., 2008, ApJ, 688, L75
- Watkins L. L., Evans N. W., An J. H., 2010, MNRAS, 406, 264 (WEA)
- White S. D. M., 1981, MNRAS, 195, 1037
- Wilkinson M. I., Evans N. W., 1999, MNRAS, 310, 645